American Mineralogist, Volume 88, pages 1679–1688, 2003

Hydromaghemite, an intermediate in the hydrothermal transformation of 2-line ferrihydrite into hematite

VIDAL BARRÓN,[1,*] JOSÉ TORRENT,[1] AND EDDY DE GRAVE[2]

[1]Departamento de Ciencias y Recursos Agrícolas y Forestales, Universidad de Córdoba, Apdo.3048, 14080 Córdoba, Spain
[2]Department of Subatomic and Radiation Physics, NUMAT Division, Ghent University, 9000 Gent, Belgium

ABSTRACT

The hydrothermal transformation of 2-line ferrihydrite into hematite proceeds slowly if a sufficient quantity of some strongly adsorbing ligand, such as phosphate or citrate, is sorbed on the starting product. In this work, we studied such transformation at temperatures ranging from 125 to 200 °C, a molar P/Fe ratio of 0–6%, and a molar citrate/Fe ratio of 3%. The products were characterized by X-ray diffraction (XRD), infrared spectroscopy, Mössbauer spectroscopy (MS) at various temperatures and in an applied field of 60 kOe, magnetic and thermal analysis, and transmission electron microscopy (TEM). At 150 °C, pure 2-line ferrihydrite transformed rapidly into hematite. The products of transformation of 2-line ferrihydrite with P/Fe = 2.75% or citrate/Fe = 3% had a magnetic susceptibility of $>240 \times 10^{-6}$ m^3/kg and were, according to XRD and MS data, mixtures of hematite with structural P, 6-line ferrihydrite, and a magnetic phase. This phase exhibited most of the characteristic reflections and MS features of maghemite, and occurred as 7–30 nm subrounded particles with lattice fringes corresponding to the maghemite (310) and (220) planes. It was designated "hydromaghemite" because it lost >3% water between 110 and ~350 °C. At 150 °C, complete transformation into hematite occurred in <120 days.

INTRODUCTION

Maghemite (γ-Fe_2O_3), a red-brown ferrimagnetic Fe oxide, has been extensively studied because of its technological importance as a recording material and a catalyst. It is also a common mineral in subtropical and tropical soils (Cornell and Schwertmann 1996) and, together with magnetite (Fe_3O_4), is responsible for the magnetic enhancement of many paleosols (Liu et al. 1992; Heller and Evans 1995; Maher 1998; Virina et al. 2000). The presence of maghemite in soils has been usually attributed to: (1) oxidation of magnetite; (2) dehydroxylation of lepidocrocite (γ-FeOOH); and (3) heating of goethite (α-FeOOH) in the presence of organic matter.

Recently, Barrón and Torrent (2002) have shown that a ferrimagnetic phase, considered to be an unusual form of maghemite, can form from 2-line ferrihydrite (a common precursor of goethite and hematite in soils) at temperatures <150 °C under oxidizing conditions. These authors have also suggested that the enhancement of magnetic properties of both Earth and Mars soils can be explained by the presence of a maghemite phase formed in this pathway. Maghemite is indeed considered to be the most likely candidate to explain the magnetism on the Martian surface (Madsen et al. 1999). The next Mars missions scheduled by the NASA and ESA will try to land rovers carrying a panoramic camera, thermal infrared and alpha-proton-X-ray equipment, and a miniaturized Mössbauer spectrometer (Klingelhöfer 1998) to identify the Fe phases constituting the Martian soils. These missions therefore justify the need to investigate in the laboratory the possible formation mechanisms of magnetic phases, in particular maghemite, as a guide to interpret the observations made on the surface of our neighbor planet.

The main objective of this work was to characterize in detail the properties of the unusual maghemite derived from the thermal transformation of 2-line ferrihydrite in the presence of some additives that retard transformation to hematite. We discuss the hypothesis that this intermediate phase can be considered as "hydromaghemite," in analogy to hydrohematite (Wolska 1981). The precursor 2-line ferrihydrite possesses a structure based on hexagonal (ABAB) and cubic (ABC) stacking of close-packed layers of O^{2-} and OH^- (Janney et al. 2000), a feature that might favor maghemite formation.

MATERIALS AND METHODS

Synthesis

Suspensions of 2-line ferrihydrite were prepared by precipitating 0.01 *M* $Fe(NO_3)_3$ with 1 *M* KOH to a final pH of 7. The initial solution contained phosphate (values of P/Fe atomic ratio in the 0–6% range) or citrate (citrate/Fe molar ratio = 3%), and are hereafter referred to as P/FeX or Cit/FeX (with X being atomic or molar ratio expressed as a per cent value). The suspensions were aged at 125 °C or higher temperatures in Polytetrafluoroethylene (PTFE)-lined vessels over periods of 0.2 to >180 days. Suspensions of 6-line ferrihydrite were prepared according to Schwertmann and Cornell (2000). After precipitation, phosphate was added to obtain values of the P/Fe atomic ratio in the 0–5% range. The suspensions of 6-line ferrihydrite with sorbed P were aged at 175 °C in PTFE-lined vessels. The synthesized products were washed free of salts by centrifuging the suspension at an acceleration of 1.5×10^4 m/s^2, discarding the supernatant, and resuspending and dialyzing the sediment in deionized water until the electrical conductivity of the equilibrium solution was <0.01 dS/m.

* E-mail: cr1balov@uco.es

Finally, the suspensions were freeze dried.

A thermal treatment (300, 500, and 700 °C for 2 h) was applied to samples with P/Fe = 2.75% and Cit/Fe = 3% prepared from 2-line ferrihydrite at 150 °C and periods of two weeks and ten days, respectively. The sample with P/Fe = 3% (prepared at 150 °C, aging time of three days) was treated with 0.2 *M* NH_4-oxalate at pH = 3 for 2 h in the dark to remove residual ferrihydrite (Schwertmann 1964). This procedure was also used to determine oxalate-soluble Fe. Total Fe (Fe_t) of the samples was considered to be the amount of Fe dissolved in 6 *M* HCl. Iron in solution was determined by atomic absorption spectrophotometry.

Mineralogical analysis

Powder X-ray diffraction (XRD) patterns were obtained with a Siemens D5000 diffractometer with monochromatized Co*K*α radiation, a step size of 0.05 °2θ, and a counting time of 20 s. Infrared (IR) spectra of KBr pellets (0.5% sample) were recorded from 380 to 4000 cm^{-1} with a Perkin-Elmer 2000 FTIR spectrometer using 4 cm^{-1} resolution and an average of 100 scans. Small portions of the synthesized products were dispersed in water and this suspension was deposited onto a holey carbon-coated copper grid before examination with a JEOL JEM-200CX or a JEOL JEM-2000EX (for high resolution) transmission electron microscope (TEM). Simultaneous thermogravimetric and differential thermal analyses (TGA-DTA) were performed in a Setaram instrument with the temperature range set at 30–800 °C, collected at a heating rate of 5 °C/min in an Ar atmosphere. Magnetization curves were obtained with a pendulum-type magnetometer (Manics DSM-8) at room temperature and the magnetic susceptibility, χ, was measured at 10^{-4} T on a Physical Property Measurement System (Quantum Design). Mössbauer spectra (MS) at various temperatures in the range 13–300 K were recorded using a time-mode spectrometer with a constant-acceleration drive and a triangular reference signal. All absorbers were prepared by mixing an amount of material with very pure carbon to achieve a homogeneous thickness of approximately 10 mg Fe/cm^2. The spectrometer was calibrated using the room-temperature spectrum of a standard hematite (which was commercial hematite powder annealed at 1000 °C and sealed-off from the atmosphere, with a absorber thickness of 2 mg Fe/cm^2). The latter itself was calibrated by means of a laser interferometer. An external field of 60 kOe parallel to the direction of the incident γ-rays was applied at 4.2 K. For these measurements, the calibration spectra were recorded simultaneously using another source and counting electronics at the opposite end of the transducer. Center shifts are quoted relative to metallic iron at room temperature.

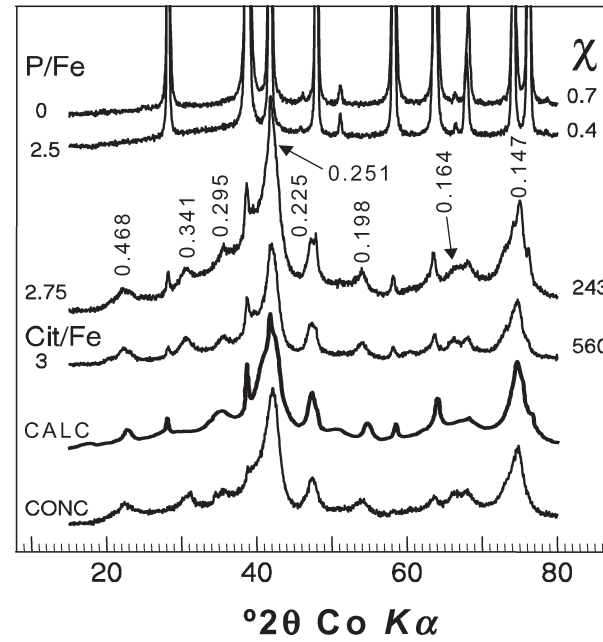

FIGURE 1. X-ray diffraction (XRD) patterns of the products synthesized at 150 °C for 2 weeks as a function of the P/Fe atomic ratio (P/Fe = 0, 2.5, 2.75%) or citrate/Fe ratio (Cit/Fe = 3%). CALC is the XRD curve calculated for a mixture of maghemite, 6-line ferrihydrite, and hematite. CONC is the experimental XRD curve for sample Cit/Fe3 after concentration with a neodimiun magnet. Numbers in labels correspond to the ligand/Fe ratio expressed as percentage. Numbers on the peaks correspond to the *d*-spacing in nm for the maghemite phase. The magnetic susceptibility, χ, (in 10^{-6} m^3/kg units) for each product is shown to the right of each pattern.

RESULTS AND DISCUSSION

Products synthesized in the presence of phosphate and citrate

Hematite. At low (≤2.5%) P/Fe ratios, the phosphated 2-line ferrihydrite aged at 150 °C for 2 weeks was completely transformed into hematite (as checked by JCPDS 13–534). TEM images show that the hematite crystals exhibit a rhombohedral habit with size between 70 and 100 nm. The sharp lines in the XRD pattern for samples with P/Fe = 0 and 2.5% (Fig. 1) are consistent with the particle sizes observed with the TEM. The *c* unit-cell edge length increased from 1.3734 nm for the P-free sample (P/Fe0) to 1.3803 nm for the P/Fe2.5 phosphated hematite; the ratio between the intensities of the 104 and 113 X-ray reflections decreased at the same time from 3.32 to 2.98. These structural changes are consistent with the ability of hematite to structurally incorporate P (Gálvez et al. 1999) and OH (Wolska 1981; Stanjek and Schwertmann 1992)

On increasing P/Fe from 0 to 2.5%, the following changes in the Mössbauer spectra recorded at 80 K were observed: the average hyperfine field, $\bar{H}_{hf}$, decreased from 537 to 528 kOe; the quadrupole shift, $2\varepsilon_Q$, dropped from 0.40 to –0.18 mm/s; and the isomer shift, δ, remained constant at 0.48 mm/s. The values of $2\varepsilon_Q$ indicate that P/Fe2.5 is in the weakly ferromagnetic (WF) state (which exists above the Morin transition temperature, T_M), whereas P/Fe0 is in the antiferromagnetic (AF) state (which exists below T_M) (De Grave et al. 1988; Vandenberghe et al. 2000). Then, the low value of $\bar{H}_{hf}$ of P/Fe2.5 relative to that of P/Fe0 can be explained by the large drop (~8 kOe) in the $\bar{H}_{hf}$ of pure hematite when it goes from below to above T_M (van der Woude 1966). Because the size of the two hematites is similar, this change only can be attributed to crystal defects caused by structural P and OH and to the relatively drastic increase of the unit-cell parameter *c* when P is incorporated in the hematite structure (Van San et al. 2001; da Costa et al. 2002; Dang et al. 1998, and references therein). Also, the FTIR spectra (not shown) reflect differences: relative to P/Fe0, the P/Fe2.5 sample exhibits stronger absorption bands at ~3400 cm^{-1}, which correspond to the stretching mode of the OH groups (Farmer 1975), and an unusual band at 700 cm^{-1}, which can be assigned to an Fe-OH vibration associated with absorbed water and hydroxyl (see discussion below). The P/Fe2.5 hematite also exhibited five weak, but distinctive bands at 935, 970, 1005, and 1100 cm^{-1}, which are assigned to P-O and P-OH vibrations (Gálvez et al. 1999; Stachen et al. 1999).

"Hydromaghemite." On increasing the P/Fe ratio of the initial 2-line ferrihydrite from 2.5% to 2.75% in the samples synthesized at 150 °C for 2 weeks (samples with P/Fe>2.75% needed longer times to crystallize), the magnetic susceptibility, χ, increased abruptly from 0.4×10^{-6} m^3/kg for P/Fe2.5 to 243×10^{-6} m^3/kg for P/Fe2.75, suggesting the presence of a

ferrimagnetic phase in the latter sample. The XRD pattern of the P/Fe2.75 sample showed the reflections of hematite (in ~6% proportion if calibrated against P/Fe2.5, which is considered to be 100% hematite) plus several characteristic reflections of cubic maghemite, such as those at 0.295 nm (220), 0.251 nm (311), and 0.147 nm (440) (Fig. 1). In contrast to typical cubic or tetragonal maghemite, this phase does not exhibit the 0.209 nm peak corresponding to the (400) reflection. Furthermore, weak and relatively broad extra lines at 0.468, 0.341, 0.225, 0.198, 0.164, and 0.151 nm are present (Fig. 1). These reflections cannot be indexed on the basis of the inverse spinel structure. Maghemite obtained from the oxidation of magnetite often displays superstructure as a result of vacancy ordering on the octahedral sites (Van Oosterhout and Rooijmans 1958; Greaves 1983; Shmakov et al. 1995), in association with a lowering of symmetry from cubic to tetragonal. This ordering gives rise to additional diffraction peaks characteristic of tetragonal maghemite (JCPDS 25-1402). The extra XRD reflections observed for the present samples, however, do not match these superstucture reflections of tetragonal maghemite, nor can they be associated with any known Fe oxyhydroxide with the exception of 6-line ferrihydrite. Compared with data obtained by Towe and Bradley (1967) for synthetic 6-line ferrihydrite, the reflections depicted in Figure 1 are narrower and better defined.

A similar XRD pattern was obtained when, instead of phosphate, citrate was used (10 days, 150 °C; see Fig. 1, sample Cit/Fe3). The χ of the product obtained with citrate (560×10^{-6} m^3/kg) was significantly higher than the χ of the P-product, and also higher than $400–450 \times 10^{-6}$ m^3/kg, which is the value usually reported for maghemite (Mullins 1977). The χ value of the pure magnetic phase could not be ascertained because none of the products obtained at different temperatures and P/Fe and Cit/Fe ratios was free of hematite, 6-line ferrihydrite, and residual 2-line ferrihydrite.

A simulated XRD pattern (Fig. 1, CALC) obtained by combining three components [viz. hematite, $R\bar{3}c$ (Blake et al. 1966); maghemite, $P4_332$ (Shmakov et al. 1995); and 6-line ferrihydrite, $P\bar{3}1$ (Drits et al. 1993)], showed a reasonable match with the observed pattern. According to this match, three phases might be present in the resulting products. The magnetic concentration (using a neodimiun hand magnet) of a dispersed suspension of the products was only able to remove most of the hematite (Fig. 1, CONC). Therefore, it is suggested that the magnetic product, hereafter named "hydromaghemite" (because it releases H_2O on heating, as discussed later), was intimately mixed, and could not be physically separated from 6-line ferrihydrite.

Water has been suggested to be essential in the formation of maghemites leading to a "hydrogen" maghemite (Braun 1952; Swaddle and Oltmann 1980; Goss 1988), analogous to lithium ferrite ($LiFe_{2.5}O_4$, with H substituting for Li). However, evidence for the presence of structural H could not be put forward (Greaves 1983). It must be pointed out that the maghemites studied by these authors were derived from different precursors. A hydrated/hydroxylated Fe oxide, such as 2-line ferrihydrite, might thus transform into hydromaghemite. An MS study of maghemite obtained from lepidocrocite (de Bakker et al. 1991) suggested that the presence of structural hydroxyl in the maghemite structure couldn't be dismissed *a priori*.

The TEM images of the P/Fe2.75 sample showed isolated hexagonal platelets of hematite (identified by selected area electron diffraction) and homogeneous subrounded particles between 7 and 30 nm in size (Fig. 2a), but no traces of the typical 2–4 nm 2-line ferrihydrite particles. Lattice fringes corresponding to hematite (012) planes (spacing of 0.37 nm), and hydromaghemite (310) and (220) planes (spacings of 0.27 and 0.29 nm, respectively) are shown in Figures 2b and 2d. The 0.25 nm spacings (Fig. 2c) could not be assigned unequivocally to any species because they may correspond to hematite (110), maghemite (311), or 6-line ferrihydrite (110) planes. In summary, the TEM images did not allow a distinction between hydromaghemite and 6-line ferrihydrite. The small size of the subrounded particles that constitute most of this sample may explain their significant solubility in oxalate ($Fe_o/Fe_t = 0.21$). The oxalate treatment did not result in changes in the relative area of the XRD reflections assigned to the two phases. It can then be argued that the two phases consist of particles similar in size and solubility, a hypothesis that is consistent with the difficulty in distinguishing them under the TEM.

A key signature of this so-called hydromaghemite is provided by the MS of the sample with P/Fe = 2.75% recorded at selected temperatures (Fig. 3). Besides a weak sextet attrib-

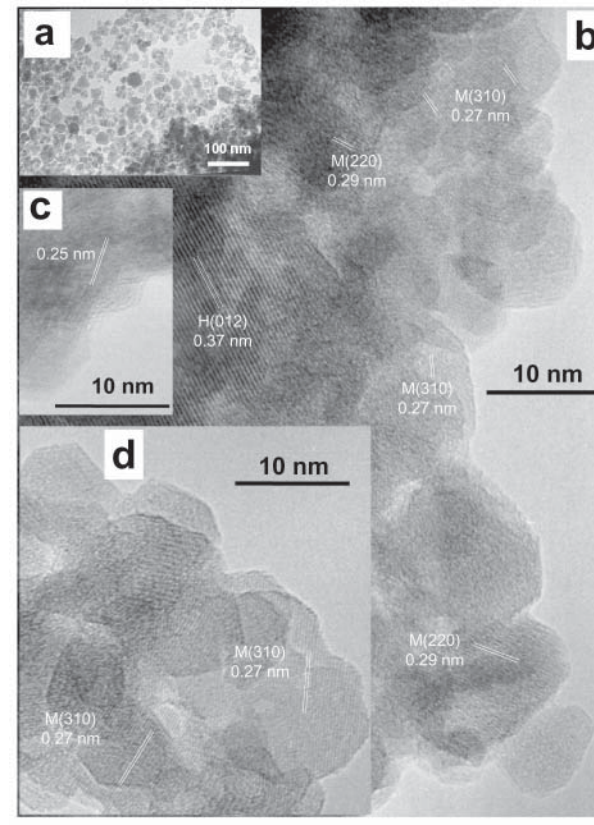

FIGURE 2. Transmission electron micrographs of P/Fe2.75 synthesized at 150 °C for 2 weeks: (**a**) typical subrounded particles of the product; (**b**) lattice fringes of hematite and maghemite; (**c**) unassigned lattice fringes (0.25 nm spacing), and (**d**) lattice fringes of maghemite.

uted to the hematite impurity, with an average contribution of ~6 %, in agreement with the XRD results, one can observe a progressive development of magnetic ordering as reflected in the evolution of the doublet, obtained at room temperature, to a very clear, but, broad sextet at 13 K. Such a behavior is supposedly typical for superparamagnetic relaxation of the atomic spins (Mørup 1987) in small-particle magnets and, consequently, is consistent with the observed nanometric size and with the high- and low-frequency susceptibility data of similar samples (Barrón and Torrent 2002).

The small particle sizes of the Fe phases constituting the P/Fe2.75 specimen also result in an asymetric shape of its MS due to distributions of the hyperfine-field values. Therefore, model-independent hyperfine-parameter distributions were used to analyze the spectra instead of a more conventional fitting procedure based on Lorentzian-shaped six-line patterns (Wivel and Mørup 1981; da Costa et al. 1995). The separation of the 6-line ferrihydrite component from that due to maghemite from the experimental data shown in Figure 3 remained, however, not feasible. Therefore, the MS were fitted with a superposition of one broad hyperfine-field distribution accounting for the unresolved maghemite and ferrihydrite contributions, a narrow distribution for hematite, and a quadrupole-splitting distribution. The quadrupole shifts for the broad magnetic component were forced to be zero, which is what is expected and evidenced to be true for maghemite. For ferrihydrite, a small non-zero quadrupole shift might be displayed in the Mössbauer spectra. However, an explanation for its existence has not been reported so far. In any case, forcing $2\varepsilon_Q = 0$ for the broad magnetic component would have no implication whatsoever upon the relevant results that can be extracted from these rather structureless line shapes. The solid lines in Figure 3 reproduce the fitted components and their sum, and relevant Mössbauer parameters are listed in Table 1. At this point it is worthwhile to mention that the hyperfine data for citrated hydromaghemite (Cit/Fe3, MS not shown) are very similar to those for the phosphated maghemite. However, it must be admitted that, although the fits to the spectra reproduced in Figure 3 are reasonably adequate, these data are rather uncertain. Consequently, trying to interpret their observed temperature variations in terms of physical models has little sense, and only a few qualitative trends can be inferred.

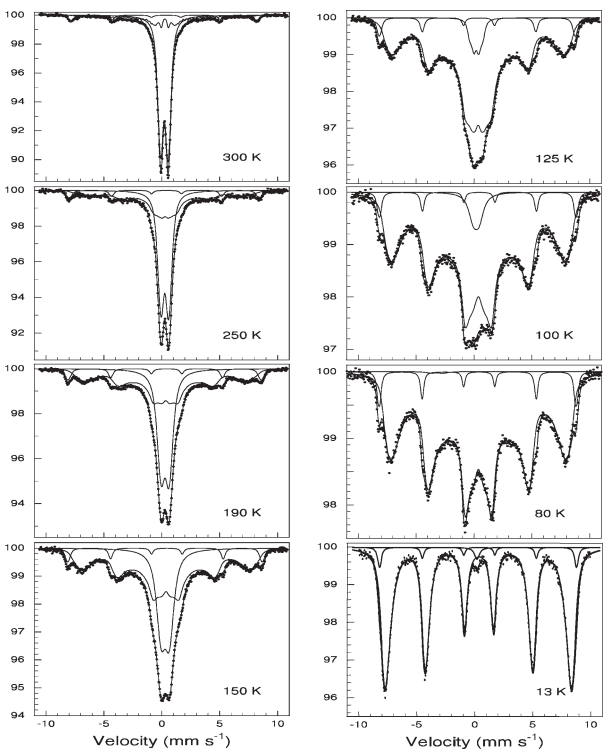

FIGURE 3. Mössbauer spectra of P/Fe2.75 at selected temperatures. Dots represent the experimental data and continuous lines the calculated subspectra and their sum.

The parameter values for the hematite subspectrum at 80 K are close to those observed for sample P/Fe2.5, which does not contain hydromaghemite. The data of Table 1 further indicate that the weakly ferromagnetic spin structure persists down to the lowest applied temperature of 13 K, although the slight decrease in the magnitude of the quadrupole shift might suggest that part of the hematite has passed through the Morin transition. However, since the hematite contribution is very low, and since the overlap of the two sextet components is considerable at low temperatures, sound conclusions in that respect cannot be drawn. In any case, the results referring to the hematite phase indirectly confirm the presence of structural P.

As a consequence of the clearly asymmetric shape of the derived hyperfine field, distributions for the maghemite + ferrihydrite components (not shown), particularly at intermediate temperatures in the double-to-sextet transition interval, the average hyperfine field ($\bar{H}_{hf}$) and the maximum-probability hyperfine fields (H^m_{hf}) differ appreciably. As expected, both these hyperfine fields increase with decreasing temperature. The values for these fields at 13 K (see Table 1) are considerably lower than the saturation values reported by da Costa et al. (1995) for nano-sized maghemite made from lepidocrocite, viz., 506 and 523 kOe, respectively. A reason for these lower values is not obvious. Perhaps the incorporation of H_2O/OH^- in the maghemite structure can account for these low field values.

As demonstrated convincingly by da Costa et al. (1995, 1998), acceptable resolution of the A- and B-site sub-sextets of nano-sized maghemites can be obtained only if an intense external magnetic field is used. The MS of sample P/Fe2.75 at 4.2 K in a longitudinal external field of 60 kOe (Fig. 4, with inset showing the derived probability distribution of the effective hyperfine fields) clearly illustrates the separation of the A- and B-site components of the present maghemite phase, with the most splitted sextet being due to tetrahedral (A) Fe^{3+}.

Fitting of this applied-field MS was not straightforward. XRD and zero-field MS have shown that a small fraction (~6%) of hematite is present in the involved sample. Therefore a hematite component with a relatively narrow effective-hyperfine-field distribution was considered with initial conditions fixed at values obtained from earlier interpretations of the external-field MS of various hematites with presumably morphological characteristics similar to those of the present hematite phase (Bowen and De Grave 1995; Van San 2001). Moreover, it is well known that maghemite, being a ferrimagnetic spinel fer-

TABLE 1. Temperature dependence of the hyperfine parameters of sample P/Fe2.75

	Hydromaghemite							Hematite			
	Sextet				Doublet			Sextet			
T(K)	$\bar{H}_{hf}$* (kOe)	H_{hf}^{m}† (kOe)	δ‡ (mm/s)	RA§ (%)	ΔE_Q‖ (mm/s)	δ‡ (mm/s)	RA§ (%)	$\bar{H}_{hf}$* (kOe)	$2\varepsilon_Q$# (mm/s)	δ‡ (mm/s)	RA§ (%)
300	229	–	0.37	20	0.67	0.33	73	499	–0.19	0.38	7
250	256	400	0.39	45	0.70	0.37	48	508	–0.20	0.41	6
190	208	440	0.44	62	0.75	0.37	30	516	–0.16	0.43	8
150	231	450	0.47	73	0.75	0.36	20	519	–0.16	0.46	7
125	275	464	0.48	83	0.67	0.23	10	524	–0.16	0.47	6
100	322	473	0.49	94	0.50	0.01	2	528	–0.16	0.49	4
80	352	474	0.49	94	0.71	0.07	1	528	–0.15	0.49	5
13	490	503	0.47	94	0.00	0.32	1	528	–0.11	0.47	5

* Average hyperfine field.
† Field of maximun probability.
‡ Isomer shift vs. α-Fe.
§ Relative area of the resolved components.
‖ Quadrupole splitting.
Quadrupole shift.

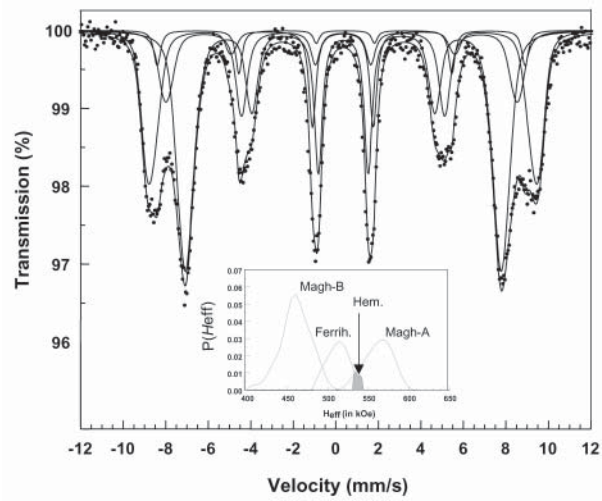

FIGURE 4. Mössbauer spectrum of P/Fe2.75 in a longitudinal external magnetic field of 60 kOe at 4.2 K. The derived distribution profiles for sextets are shown as an inset.

rite, has its octahedral and tetrahedral absorption lines shifted on applying an external field, respectively to lower and higher absolute velocities, which is clearly reflected in the MS depicted in Figure 4. So, at least two maghemite components are required to interpret the spectra. However, using a superposition of three distributed components led to unacceptable results in that the probability distribution profile $p(H_{eff})$ of the B-site effective hyperfine field is calculated to be bimodal, with an obvious, though weaker, maximum at ~515 kOe. This result would mean that a fraction of the B-site Fe^{3+} ions would experience a hyperfine field of ~570 kOe, which is beyond any doubt unreasonably high for Fe^{3+} in an oxidic spinel (Vandenberghe and De Grave 1989). Therefore, a fourth distributed component with field range 480–540 kOe, attributable to antiferromagnetic ferrihydrite, was introduced, yielding significantly better fits and Mössbauer parameters (see Table 2) that are within expectations for the constituent Fe phases. However, a few constraints had to be imposed in order to arrive at a convergent fit.

TABLE 2. Hyperfine parameters for sample P/Fe2.75 recorded at 4.2 K in an applied field of 60 kOe

	Hydromaghemite		6-line	Hematite
	A	B	Ferrihydrite	
$\bar{H}_{eff}$* (kOe)	562	460	511	537
H_{eff}^{m}† (kOe)	568	459	514	534
$2\varepsilon_Q$# (mm/s)	0	0	–0.07	–0.2
δ‡ (mm/s)	0.45	0.47	0.43	0.48
A1:A2‖	3:0.33	3:0.77	3:2.97	3:3.50
RA§ (%)	27	48	20	5

* Average effective hyperfine field.
† Effective field of maximun probability.
# Quadrupole shift.
‡ Isomer shift vs. α-Fe.
‖ Ratio between the areas of lines 1 and 2.
§ Relative area of the resolved components.

The area ratio *A*1/*A*2 of the outer to middle lines (1 and 2) in the applied-field MS is close to unity for the ferrihydrite component. This means that the atomic spins are to some extent ordered along a preferred orientation with respect to the external field and not in a random direction, which would indeed yield an area ratio of 3:2. The average angle of the effective hyperfine field with respect to the external field, calculated from the well-known and simple expression that relates *A*1/*A*2 to the angle between the magnetic hyperfine field and the propagation vector of the incident γ-rays, is ~67°. From this value, combined with the observed average effective field of 511 kOe (see Table 2), one calculates a hyperfine field of H_{hf} = 491 kOe, which falls well within the range of field values measured for various ferrihydrites (Murad and Schwertmann 1980).

The Mössbauer parameters for the maghemite subspectra are comparable to those of the poorly crystalline maghemites examined by da Costa et al. (1998), in which the middle lines (2 and 5) in the MS do not vanish. The ratio A1/A2 were found to be 3:0.33 and 3:0.77 for the A- and B-sites, respectively, as opposed to a 3:0 ratio as expected for an oriented collinear ferrimagnet like bulk maghemite. Hence, the spin arrangement in the present maghemite phase is not collinear with respect to the external field thus giving rise to a canted magnetic structure (Coey 1971; da Costa et al. 1998). The spin-canting angles can be estimated from the intensity ratios A1/A2 (see Table 2) according to a simple expression that relates these ratios to the angle between the magnetic hyperfine field and the propaga-

tion vector of the incident γ-rays. These angles are 23° and 145° for A and B sites, respectively, for the present maghemite phase. However, the true physical meaning of these angles is not straightforward. It has been shown (de Bakker et al. 1991) that the applied-field MS of small-particle maghemite cannot be described merely by distributions of effective-hyperfine fields, but that, in addition, broad distributions, uncorrelated with the magnitudes of the fields, for the respective canting angles need to be considered. Only in that case can meaningful data concerning the cantings for the two sublattice spins be derived. Nevertheless, the values reported in the present work are believed to be indicative of the degrees of canting. Moreover these values are similar to the ones obtained by da Costa et al. (1998) for poorly crystalline nanosized maghemite powders made from lepidocrocite, for which the applied-field MS were fitted with a two-parameter distribution approach. Such an approach cannot be applied for the present MS of the hydromaghemites, taking into account the presence of the additional, strongly overlapping spectral components.

Additional information about the nature of the products studied can be drawn from the FTIR spectra (not shown). Both P/Fe2.75 and Cit/Fe3 exhibit a very intense and broad band in the 3400 cm^{-1} region and a well-defined band at 1620 cm^{-1}, both of which correspond to OH groups. Both the hydro-P-hematite (P/Fe2.5) and the P/Fe2.75 products show similar weak bands near 1000 cm^{-1} that can, as mentioned above, be assigned to P-O vibrations. The Cit/Fe3 sample has a band at 1380 cm^{-1}, typical of C-O vibrations. The band at 700 cm^{-1}, attributed to Fe-OH vibrations, of this hydromaghemite is similar to the common band of Fe-O vibrations at 570 and 440 cm^{-1}.

Time course of the transformation of 2-line ferrihydrite into hydromaghemite

The XRD patterns and MS (80 K) of the products obtained successively by ageing the P/Fe3% ferrihydrite at 150 °C are shown in Figure 5. According to the previous results, and in order to discriminate the precursor 2-line ferrihydrite from the superparamagnetic hydromaghemite, a temperature of 80 K was selected for the Mössbauer measurement to ensure that the latter phase is represented only as a magnetically split spectrum. Figure 5 also includes the values of Fe_o/Fe_t, i.e., the ratio of oxalate-extractable to total Fe, which is correlated with the degree of crystallinity of iron oxides (Schwertmann 1964). The values of the magnetic susceptibility, χ, are indicated as well.

The initial product P/Fe3 exhibited the characteristic features of 2-line ferrihydrite, i.e., two very broad XRD peaks, a doublet MS with a quadrupole splitting of 0.73 mm/s, high solubility in oxalate and low magnetic susceptibility (2×10^{-6} m^3/kg), thus indicating absence of ferrimagnetic phases. However, by fitting the MS by the aforementioned model-independent hyperfine field distribution, a magnetically split sextet (assigned to a maghemite-like phase) can be resolved. The area of this component (see also Table 3) increases relative to that of the doublet when the crystallinity of the products, as quantified by the lower Fe_o/Fe_t values and as reflected in the higher number of XRD lines, increases. Simultaneously, a progressive increase in the magnetic susceptibility was observed suggesting that formation of the ferrimagnetic phase is concomitant

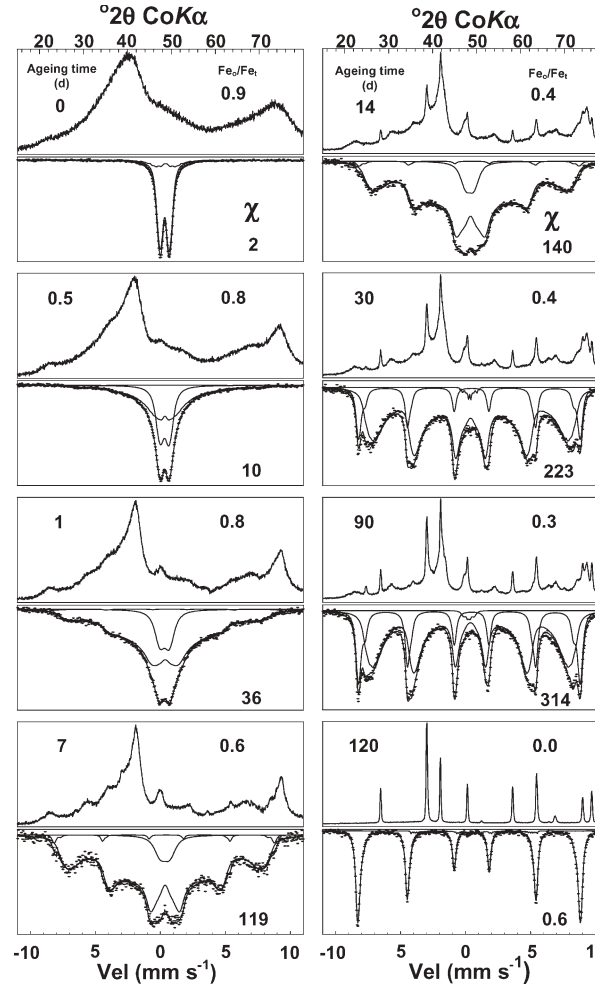

FIGURE 5. (Top) XRD pattern and (bottom) Mössbauer spectra for the successive products obtained by ageing a phosphated 2-line ferrihydrite (P/Fe = 3%) at 150 °C for 120 days. The ratio of oxalate-extractable to total Fe (Fe_o/Fe_t) and the magnetic susceptibility, χ, (in 10^{-6} m^3/kg units) for each product are shown in the upper and lower right side, respectively.

with the transformation of 2-line ferrihydrite. After 7 days, the characteristic peaks for hydromaghemite were evident in the XRD pattern overlapping with hematite lines. Both phases and 6-line ferrihydrite were also detected after 3 days of aging in the residual product obtained after dissolution the poorly crystalline matrix (85%, according to the Fe_o/Fe_t ratio) with oxalate (Fig. 6). After oxalate treatment, the characteristic XRD lines (including the extra peaks assigned to hydromaghemite) remained, the contribution of the sextet to the MS was higher, and the magnetic susceptibility had increased as a result of removal of residual 2-line ferrihydrite.

With time, both the proportions of hematite, hydromaghemite, and 6-line ferrihydrite increased steadily at the expense of the 2-line ferrihydrite, with a leveling off beyond an aging time of 7 days. For ageing times >120 days hematite was the only product. The resulting hematite exhibited the aforementioned features of the P-hydrohematite, that is, a longer *c*

TABLE 3. Aging-time dependence of the hyperfine parameters of sample P/Fe3

	Hydromaghemite Sextet				2-line ferrihydrite Doublet			Hematite Sextet			
Time (Days)	$\bar{H}_{hf}$* (kOe)	H^{m}_{eff}† (kOe)	δ‡ (mm/s)	RA§ (%)	ΔE_Q‖ (mm/s)	δ‡ (mm/s)	RA§ (%)	$\bar{H}_{hf}$* (kOe)	$2\varepsilon_Q$# (mm/s)	δ‡ (mm/s)	RA§ (%)
0	111	69	0.51	12	0.73	0.45	88	–	–	–	0
0.5	154	59	0.46	60	0.72	0.44	40	–	–.	–	0
1	241	115	0.48	84	0.74	0.44	15	521	–0.14	0.79	1
7	299	463	0.37	90	0.74	0.46	8	520	–0.16	0.49	2
14	293	466	0.49	90	0.65	0.43	8	525	–0.15	0.49	2
30	367	469	0.49	80	0.57	0.43	1	522	–0.17	0.48	19
90	414	472	0.49	69	0.56	0.35	1	522	–0.17	0.48	30
120	–	–	–	0	–	–	0	528	–0.19	0.48	100

* Average hyperfine field.
† Field of maximun probability.
‡ Isomer shift vs. α-Fe.
§ Relative area of the resolved components.
‖ Quadrupole splitting.
Quadrupole shift.

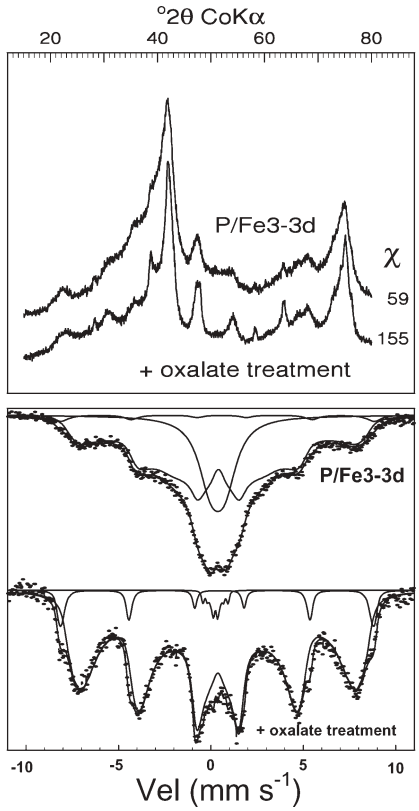

FIGURE 6. (Top) X-ray and (bottom) Mössbauer spectra for sample P/Fe3 aged for 3 days before and after oxalate treatment.

unit-cell length (1.3811 nm) and a lower I_{104}/I_{113} ratio (2.93) than the reference hematite and a quadrupole shift of –0.19 mm/s (80 K), indicating a weakly ferromagnetic behavior.

The fact that hydromaghemite and 6-line ferrihydrite exhibit similar behavior regarding the kinetics of their transformation into hematite, their solubility in oxalate, and, apparently, particle size is intriguing. One can speculate that the XRD and MS data also are consistent with the presence of one single phase showing both maghemite and 6-line features. However, our attempts to adapt these data to different structures were unsuccessful and deserve indeed consideration in the future.

The transformation of phosphated and citrated ferrihydrites aged during different times was monitored quantitatively by measuring the magnetic susceptibility, χ, of samples kept at different temperatures. The results are shown in Figure 7. In all cases, χ increased gradually and then decreased rapidly as the likely result of fast transformation of the intermediate ferrimagnetic products into hematite. The intermediate products exhibited higher χ for the citrate- than in the phosphate-containing systems.

In summary, a genetic relationship exists between 2-line ferrihydrite and the mixture of hydromaghemite and 6-line ferrihydrite. The hypothesis that 2-line transforms into 6-line ferrihydrite was dismissed by some authors (Schwertmann et al. 1999; Janney et al. 2000). However, Rancourt et al. (2001) found some evidence for such a transformation when 2-line ferrihydrite was doped with As. It must be noted that the present results seem to support indirectly the idea of the possible existence of tetrahedral Fe in 2-line ferrihydrite (which would favor maghemite formation). This controversial subject has attracted attention in the recent past (Jambor and Dutrizac 1998, and references therein). Extended X-ray absorption fine structure (EXAFS) and Fe X-ray absorption near-edge structure (XANES) spectroscopic studies seem to indicate that no tetrahedral Fe is present in ferrihydrite (Manceau and Gates 1997). In contrast, Eggleton and Fitzpatrick (1988) and Zhao et al. (1994) concluded from their XRD, EXAFS, and XANES measurements that Fe occurs in both tetrahedral and octahedral coordination in ferrihydrite. These contrasting results may reflect the fact that the samples used were in different stages of their transformation to a more-or-less developed maghemite-like structure. Recent nanodiffraction studies (Janney et al. 2000, 2001) have suggested that, in contrast to 6-line ferrihydrite, 2-line ferrihydrite partly possesses a maghemite-like structure. In fact, when 6-line ferrihydrite was aged with different amounts of sorbed P, no ferrimagnetic phases were obtained in detectable amounts, with hematite or mixtures of hematite and goethite being the final products (results not shown). This finding is consistent with the results obtained by Mazzetti and Thistlethwaite (2002), who used Raman spectroscopy to show that, under heating by the He-Ne laser beam, 2-line ferrihydrite transformed into hematite via a maghemite intermediate whereas

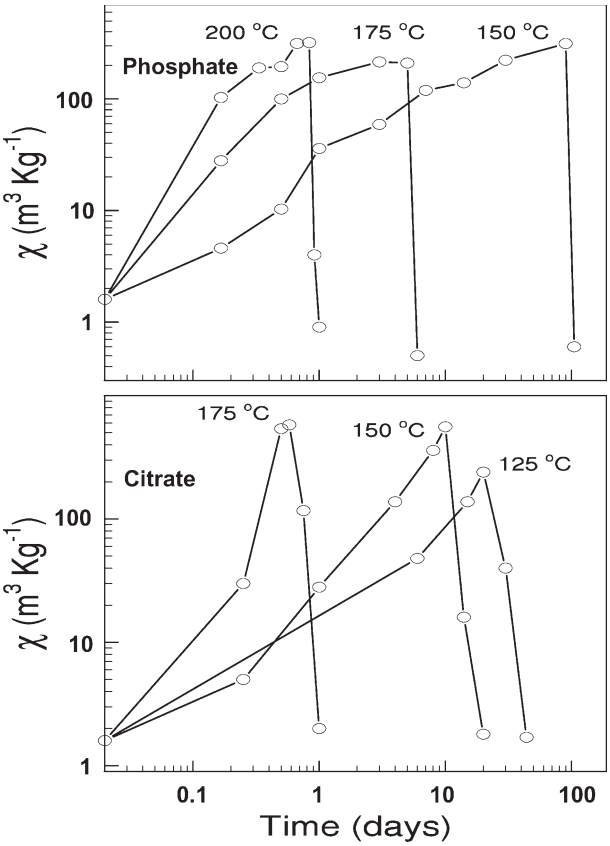

FIGURE 7. Magnetic susceptibility as a function of ageing time for the products formed from phosphated (top) and citrated ferrihydrite (bottom), with a ligand/Fe ratio of 3% at different temperatures.

6-line ferrihydrite transformed directly into hematite.

A tentative mechanism of the transformation of ferrihydrite can be proposed on the basis of the presently and previously reported data. If a sufficient amount of a strongly adsorbing ligand such as phosphate or citrate (ligand/Fe ≈ 3%) is present, the ligand can cover the spherical particles of fresh ferrihydrite and, as such, delay the aggregation that precedes hematite formation. However, rearrangement and internal crystallization of these ligand-coated and isolated spheres of ferrihydrite is not necessarily hindered and, with time and an appropriate temperature, a relatively well-structured hydromaghemite eventually can be produced. The hypothetical presence of tetrahedral Fe in 2-line ferrihydrite might thus favor this process.

Thermal behavior of the products of transformation

Typical examples of thermogravimetric curves for both phosphated and citrated hydromaghemites are presented in Figure 8a. They clearly exhibit three regions. A weight loss of ~3% for Cit/Fe3 and ~5% for P/Fe2.75 can be attributed to easily desorbable surface water. The weight loss of ~5.8% between 110 and 330 °C (for Cit/Fe3) or 390 °C (for P/Fe2.75) can be due to the dehydroxylation reaction of the hydromaghemite and 6-line ferrihydrite. Finally, the gradual weight loss beyond these temperatures is believed to be associated with the hydrohematite. If, according to the MS data, one assumes that the proportion of 6-line ferrihydrite in these products is ~20% and ferrihydrite contains on average ~12% water (Jambor and Dutrizac 1998), a simple calculation indicates that the studied hydromaghemites lost >3% water lost between 110 and ~350 °C, thus justifying the term used for them.

The continuous loss of OH was also evident from the FTIR spectra for sample P/Fe2.75 (not shown) because the intensity of all bands related to OH vibrations (3400, 1620 and 700 cm^{-1}) decrease significantly. The DTA curve (Fig. 8b) shows the low-temperature endothermic peak corresponding to the loss of water and several exothermic peaks. Conversion to hematite can be related to the peak at about 490 °C for the citrated sample and at a higher temperature for the phosphated one. This increase in the temperature of transformation of P-maghemite to P-hematite relative to pure maghemite was reported by Tronc and Jolivet (1986) and Torrent and Barrón (2000). Additional exothermic peaks, more clearly defined for Cit/Fe3 than for P/Fe2.75, are observed between 220 and 320 °C. Towe and Bradley (1967) obtained two similar peaks (at about 275 °C) for synthetic 6-line ferrihydrite but did not discuss the nature of this exothermic reaction. The XRD patterns of phosphated and citrated samples heated at 300 °C (not shown) did not exhibit the reflections at 0.468, 0.341, and 0.164 nm (assigned to hydromaghemite). Therefore, the exothermic peaks might be due to a phase transformation involving OH loss and

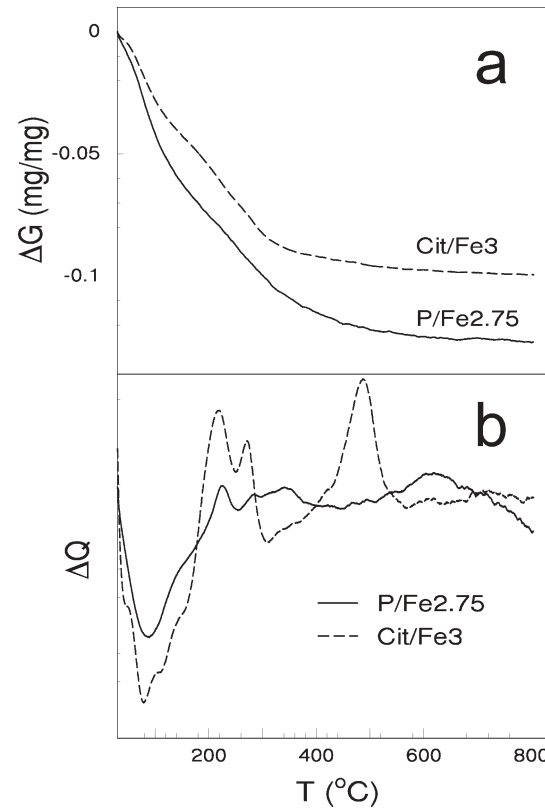

FIGURE 8. Thermogravimetric (**a**) and differential thermal analysis (**b**) curves for hydromaghemites Cit/Fe3 and P/Fe2.75.

crystallinity changes in hydromaghemite.

The thermal transformation of hydromaghemite is accompanied by significant changes in magnetic behavior. The magnetization vs. magnetic field curves at room temperature for the phosphated sample saturate to values that decrease with increasing temperature of treatment (Fig. 9). On heating at 300 °C, the value of χ dropped from 243 to 80×10^{-6} m^3/kg in P/Fe2.75 and from 560 to 100×10^{-6} m^3/kg in Cit/Fe3. This behavior cannot be due to transformation into hematite because the XRD patterns indicated that heat treatment resulted in little increase in the proportion of this phase (data not shown). Moreover, the zero-field MS at 80 K for the thermally treated P/Fe2.75 sample (data not shown) provided no clue to the decrease in magnetic susceptibility. Finally, in an attempt to find an explanation for the dramatic drop in magnetic susceptibility, an external-field MS was collected at 4.2 K in 60 kOe for the treated (300 °C) sample P/Fe2.75. This spectrum (Fig. 10) and the applied-field MS obtained before heating (Fig. 4) do not differ significantly in the relative spectral areas of the four components (Tables 2 and 4). Only differences in the ratio of the areas of lines 1 and 2 for maghemite are noticed. They indicate that the heated has a more pronounced spin canting than the unheated product (compare data in Tables 2 and 4). An increase in the canting for maghemite has been associated with surface effects in small particles. It also can be speculated that the spins are more rigidly bound to spatial directions and, hence, less susceptible to changes in the strength of the external field, and therefore resulting in a lower magnetic susceptibility. More work is needed to clarify these points.

ACKNOWLEDGMENTS

This work was supported by the Spanish Ministerio de Ciencia y Tecnología in the framework of project PB98-1015. V. Barrón is indebted to the Spanish Ministerio de Educación, Cultura y Deporte for a 3-month grant study period at the NUMAT Department, University of Ghent, Belgium. The Mössbauer experiments were financially supported by the Fund for Scientific Research—Flanders under grant No 3G.00007.97 to EDG.

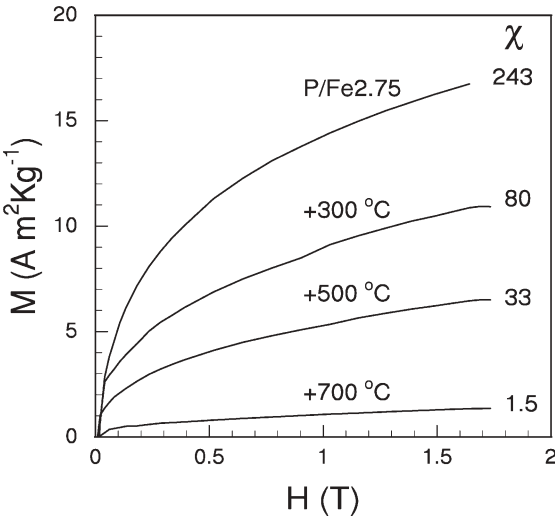

FIGURE 9. Room temperature magnetization curves of the products obtained after thermal treatment of P/Fe2.75. The magnetic susceptibility, χ, (in 10^{-6} m^3/kg units) for each product are shown to the right.

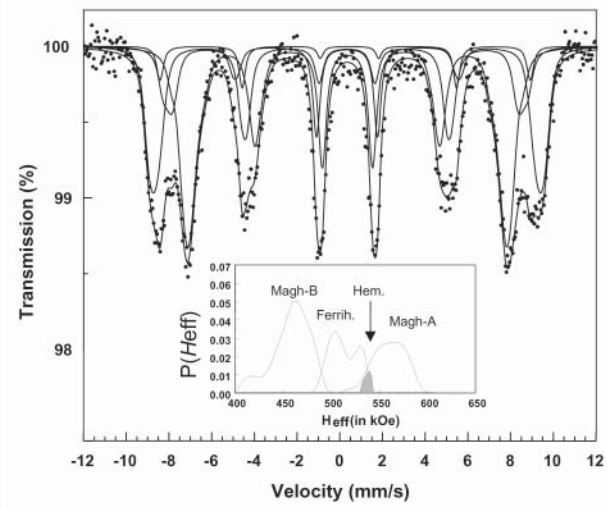

FIGURE 10. Mössbauer spectrum of P/Fe2.75 after heating at 300 °C in a longitudinal external magnetic field of 60 kOe at 4.2 K. The derived distribution profiles for the sextets are shown as an inset.

TABLE 4. Hyperfine parameters for sample P/Fe2.75 after heating at 300 °C recorded at 4.2 K in an applied field of 60 kOe

	Hydromaghemite		6-line	Hematite
	A	B	Ferrihydrite	
$\bar{H}_{eff}$* (kOe)	560	458	513	538
H^{m}_{eff}† (kOe)	567	462	504	539
$2\varepsilon_Q$# (mm/s)	0	0	–0.05	–0.2
δ‡ (mm/s)	0.45	0.44	0.43	0.47
A1:A2‖	3:0.46	3:1.11	3:2.85	3:3.50
RA§ (%)	27	44	24	5

* Average effective hyperfine field.
† Effective field of maximun probability.
# Quadrupole shift.
‡ Isomer shift vs. α-Fe.
‖ Ratio between the areas of lines 1 and 2
§ Relative area of the resolved components.

REFERENCES CITED

Barrón, V. and Torrent, J. (2002) Evidence for a simple pathway to maghemite in Earth and Mars soils. Geochimica et Cosmochimica Acta, 66, 2801–2806.

Blake, R.L., Hessevick, R.E., Zoltai, T., and Finger, L. (1966) Refinement of the hematite structure. American Mineralogist, 51,123–129.

Bowen, L.H. and De Grave, E. (1995) Mössbauer spectra in external field of highly substituted aluminous hematites. Journal of Magnetism and Magnetic Materials, 139, 6–10.

Braun, P.B. (1952) A superstructure in spinels. Nature, 170, 1123.

Coey, J.M.D. (1971) Non-collinear spin arrangement in ultrafine ferrimagnetic crystallites. Physics Review Letters, 27, 1140–1142.

Cornell, R.M. and Schwertmann, U. (1996) The iron oxides. Structure, properties, reactions, occurrence and uses. VCH, Weinheim.

da Costa, G.M., De Grave, E., Bowen, L.H., de Bakker, P.M.A., and Vandenberghe, R.E. (1995) Variable-temperature Mössbauer spectroscopy of nano-sized maghemite and Al-substituted maghemites. Clays and Clay Minerals, 43, 562–568.

da Costa, G.M., De Grave, E., and Vandenberghe, R.E. (1998) Mössbauer spectroscopy of magnetite and Al-substituted maghemites. Hyperfine Interactions, 117, 207–243.

da Costa, G.M., Van San, E., De Grave, E., Vandenberghe, R.E., Barrón, V., and Datas, L. (2002) Al hematites prepared by homogeneous precipitation of oxinates: Material characterization and determination of the Morin transition. Physics and Chemistry of Minerals, 29, 122–131.

Dang, M.-Z., Rancourt, D.G., Dutrizac, J.E., Lamarche, G., and Provencher, R. (1998) Interplay of surface conditions, particle size, stoichiometry, cell parameters, and magnetism in synthetic hematite-like materials. Hyperfine Interactions, 117, 271–319.

de Bakker, P.M.A., De Grave, E., Vandenberghe, R.E., Bowen, L.H., Pollard, R.J., and Persoons, R.M. (1991) Mössbauer study of the thermal decomposition of

lepidocrocite and characterization of the decomposition products. Physics and Chemistry of Minerals, 18, 131–143.
De Grave, E., Bowen, L.H., Vochten, R., and Vandenberghe, R.E. (1988) The effect of crystallinity and Al substitution on the magnetic structure and Morin transition in hematite. Journal of Magnetism and Magnetic Materials, 72, 141–151.
Drits, V.A., Sakharov, B.A., Salyn, A.L., and Manceau, A. (1993) Structural model for ferrihydrite. Clay Minerals, 28, 185–207.
Eggleton, R.A. and Fitzpatric, R.W. (1988) New data and a revised structural model for ferrihydrite. Clays and Clay Minerals, 36, 111–124.
Farmer, V.C. (1975) Infrared spectroscopy in mineral chemistry. In A.W. Nicol, Ed., Physicochemical Methods of Mineral Analysis, 357–388. Plenum Press, New York, London.
Gálvez, N., Barrón, V., and Torrent, J. (1999) Preparation and properties of hematite with structural phosphorus. Clays and Clay Minerals, 47, 375–385.
Goss, C.J. (1988) Saturation magnetisation, coercivity and lattice parameter changes in the system Fe_3O_4–γ-Fe_2O_3, and their relationship to structure. Physics and Chemistry of Minerals, 16, 164–171.
Greaves, C. (1983) A powder neutron diffraction investigation of vacancy ordering and covalence in γ-Fe_2O_3. Journal of Solid State Chemistry, 49, 325–333.
Heller, F. and Evans, M.E. (1995) Loess magnetism. Reviews of Geophysics, 33, 211–240.
Jambor, J.L. and Dutrizac, J.E. (1998) Occurrence and constitution of natural and synthetic ferrihydrite, a widespread iron oxyhydroxide. Chemical Reviews, 98, 2549–2585.
Janney, D.E., Cowley, J.M., and Buseck, P.R. (2000) Structure of synthetic 2-line ferrihydrite by electron nanodiffraction. American Mineralogist, 85, 1180–1187.
——— (2001) Structure of synthetic 6-line ferrihydrite by electron nanodiffraction. American Mineralogist, 86, 327–335.
Klingelhöfer, G. (1998) In-situ analysis of planetary surfaces by Mössbauer spectroscopy. Hyperfine Interactions, 113, 369–374.
Liu, X., Shaw, J., Liu, T., Heller, F., and Yuan, B. (1992) Magnetic mineralogy of Chinese loess and its significance. Geophysical Journal International, 108, 301–308.
Madsen, M.B., Hviid, S.F., Gunnlaugsson, H.P., Knudsen, J.M., Goetz, W., Pedersen, C.T., Dinesen, A.R., Mogensen, C.T., Olsen, M., and Hargraves, R.B. (1999) The magnetic properties experiments on Mars Pathfinder. Journal of Geophysical Research, 104, 8761–8779.
Maher, B.A. (1998) Magnetic properties of modern soils and quaternary loessic paleosols: paleoclimatic implications. Paleogeography, Paleoclimate, Paleoecology, 137, 25–54.
Manceau, A. and Gates, W.P. (1997) Surface structural model for ferrihydrite. Clays and Clay Minerals, 45, 448–460.
Mazzetti, L. and Thistlethwaite, P.J. (2002) Raman spectra and thermal transformations of ferrihydrite and schwertmannite. Journal of Raman Spectroscopy, 33, 104–111.
Mørup, S. (1987) Mössbauer effect studies of microcrystalline materials. In G.L. Long, Ed., Mössbauer spectroscopy applied to inorganic chemistry. Vol. 2. Plenum Press, New York.
Mullins, C.E. (1977) Magnetic susceptibility of the soil and its significance in Soil Science—A review. Journal of Soil Science, 28, 223–226.
Murad, E. and Schwertmann, U. (1980) The Mössbauer spectrum of ferrihydrite and its relations to those of other iron oxides. American Mineralogist, 65, 1044–1049.
Rancourt, D.G., Fortin, D., Pichler, T., Thibault, P.J., Lamarche, G., Morris, R.V., and Mercier, P.H.J. (2001) Mineralogy of a natural As-rich hydrous ferric oxide coprecipitate formed by mixing of hydrothermal fluid and seawater: Implications regarding surface complexation and color banding in ferrihydrite deposits. American Mineralogist, 86, 834–851.
Schwertmann, U. (1964) Differenzierung der Eisenoxide des Bodens durch Extraktion mit Ammoniumoxalat-lösung. Zeitschrift für Pflanzenernährung und Bodenkunde, 105, 194–202.
Schwertmann, U. and Cornell, R.M. (2000) Iron oxides in the laboratory. Preparation and characterization. VCH, Weinheim.
Schwertmann, U., Friedl, J., and Stanjek, H. (1999) From Fe(III) ions to ferrihydrite and then to hematite. Journal of Colloid and Interface Science, 209, 215–223.
Shmakov, A.N., Kryukova, G.N., Tsybulya, S.V., Chuvilin, A.L., and Solovyeva, L.P. (1995) Vacancy ordering in γ-Fe_2O_3: synchroton X-ray powder diffraction and high-resolution electron microscopy studies. Journal of Applied Crystallography, 28, 141–145.
Stachen, M., Morales, M.P., Ocaña, M., and Serna, C.J. (1999) Effect of precursor impurities on the magnetic properties of uniform γ-Fe_2O_3 ellipsoidal particles. Physical Chemistry Chemical Physics, 1, 4465–4471
Stanjek, H. and Schwertmann, U. (1992) The influence of aluminum on iron oxides. Part XVI: Hydroxyl and aluminum substitution in synthetic hematites. Clays and Clay Minerals, 40, 347–354.
Swaddle, T.W. and Oltmann, P. (1980) Kinetics of the magnetite-maghemite-hematite transformation, with special reference to hydrothermal systems. Canadian Journal of Chemistry, 58, 1763–1771.
Torrent, J. and Barrón, V. (2000) Key role of phosphorus in the formation of the iron oxides in Mars soils? Icarus, 145, 645–647.
Towe, K.M. and Bradley, W.F. (1967) Mineralogical constitution of colloidal "hydrous ferric oxides". Journal of Colloid and Interface Science, 24, 384–392.
Tronc, E. and Jolivet, J.P. (1986) Surface effects on magnetically coupled "γ-Fe_2O_3" colloids. Hyperfine Interactions, 28, 525–528.
Vandenberghe, R.E. and De Grave, E. (1989) Mössbauer effect studies of oxidic spinels. In G.J. Long and F. Grandjean, Eds., Mössbauer spectroscopy applied to inorganic chemistry, p. 59–182. Plenum Press, New York.
Vandenberghe, R.E., Barrero, C.A., da Costa, G.M., Van San, E., and De Grave, E. (2000) Mössbauer characterization of iron oxides and (oxy)hydroxides: the present state of the art. Hyperfine Interactions, 126, 247–259.
Van der Woude, F. (1966) Mössbauer effect in α-FeOOH. Physica Status Solidi, 17, 417–432.
Van Oosterhout, G.H. and Rooijmans, C.J.M. (1958) A new superstructure in Gamma-Ferric Oxide. Nature, 181, 44.
Van San, E. (2001) Mössbauer spectroscopyc study of the effects of crystallinity and aluminiun substitution on the magnetic transitions in hematite. Ph.D. thesis, University of Ghent, Gent, pp.148.
Van San, E., De Grave, E., Vandenberghe, R.E., Desseyn, H.O., Datas, L., Barrón, V., and Rousset, A. (2001) Study of Al-substituted hematites, prepared from thermal treatment of lepidocrocite. Physics and Chemistry of Minerals, 28, 488–497.
Virina, E.I., Faustov, S.S., and Heller, F. (2000) Magnetism of loess-paleosol formation in relation to soil-forming and sedimentary processes. Physics and Chemistry of the Earth, 25, 475–478.
Wivel, C. and Mørup, S. (1981) Improved computational procedure for evaluation of overlapping hyperfine parameter distribution in Mössbauer spectra. Journal of Physics E: Scientific Instruments, 14, 605–610.
Wolska, E. (1981) The structure of hydrohematite. Zeitschrift für Kristallographie, 154, 69–75.
Zhao, J., Huggins, F.E., Feng, Z., and Huffman, G.P. (1994) Ferrihydrite: surface structure and its effects on phase transformation. Clays and Clay Minerals, 42, 737–746.

MANUSCRIPT RECEIVED JULY 4, 2002
MANUSCRIPT ACCEPTED APRIL 13, 2003
MANUSCRIPT HANDLED BY DARBY DYAR